**Structural Engineering and Mechanics**, *Vol. 52, No. 1 (2014) 75-87*
DOI: http://dx.doi.org/10.12989/sem.2014.52.1.075 

# Theoretical tensile model and cracking performance analysis of laminated rubber bearings under tensile loading

Shicai Chen[*1], Tongya Wang[1a], Weiming Yan[1b], Zhiqian Zhang[1] and Kang-Suk Kim[2]

[1]*Department of Civil Engineering, Beijing University of Technology, Pingleyuan 100, Chaoyang, Beijing 100124, China*
[2]*Department of Civil Engineering, Tsinghua University, Qinghuayuan 1, Beijing 100084, China*

*(Received November 12, 2012, Revised May 30, 2014, Accepted June 20, 2014)*

**Abstract.** To analyze the tension performance of laminated rubber bearings under tensile loading, a theoretical tension model for analyzing the rubber bearings is proposed based on the theory of elasticity. Applying the boundary restraint condition and the assumption of incompressibility of the rubber (Poisson's ratio of the rubber material is about 0.5 according the existing research results), the stress and deformation expressions for the tensile rubber layer are derived. Based on the derived expressions, the stress distribution and deformation pattern especially for the deformation shapers of the free edges of the rubber layer are analyzed and validated with the numerical results, and the theory of cracking energy is applied to analyze the distributions of prediction cracking energy density and gradient direction. The prediction of crack initiation and crack propagation direction of the rubber layers is investigated. The analysis results show that the stress and deformation expressions can be used to simulate the stress distribution and deformation pattern of the rubber layer for laminated rubber bearings in the elastic range, and the crack energy method of predicting failure mechanism are feasible according to the experimental phenomenon.

**Keywords:** laminated rubber bearing; isolation; deformation; tension model; finite element method

## 1. Introduction

Recently, the high rise buildings have been built with the development of seismic isolated structures, and the large aspect ratio isolated buildings are also applied in engineering (Hino 2008), the tension stress will appear in the bearings of these kinds of structures (Takaoka *et al.* 2011) and there is a difference between design and real behavior of the base isolation device (Lee 2014), therefore, many experimental and numerical investigations have been carried out on the tensile behavior of laminated rubber bearings. Liu (2004) conducted tensile tests on the rubber bearings with diameter of 300 mm, the double stiffness model and original stiffness model are proposed to describe the tension properties of rubber isolators (Yang 2010). In order to study the tension

∗Corresponding author, Ph.D., E-mail: csc@bjut.edu.cn
[a]Ph.D. Student, E-mail: wangtongya@email.bjut.edu.cn
[b]Professor, E-mail: yanwm@bjut.edu.cn


http://www.techno-press.org/?journal=sem&subpage=8 ISSN: 1225-4568 (Print), 1598-6217 (Online)

properties of laminated rubber bearings with different shape factors, Muramatsu *et al.* (2001) carried out tests on natural rubber bearings with three types of diameter, the test results show that the tensile deformation capacity of natural rubber bearing decreases with the increase of diameter, but the reason was not analyzed and given. Zhang (2012) conducted tensile tests on the rubber bearings with diameter of 800mm to investigate the tensile performance and cracking mechanism. The stress are not easy to be measured during the tests, however, the overall performance and stress distribution can be analyzed through theory analysis method or the FEA numerical method (Matsuda 2004, Yoshida *et al.* 2004). Closed-form expressions of the compression load-deflection relation and stress distribution which satisfy exactly the governing equations and conditions, are derived by Ling (1995) using an approximate-linear approach, the results show that the compression stress distributes un-uniformly and the stress at the central part of the bearing is larger than the other region of the rubber layer. Yoshida *et al.* (2004), Matsuda (2004) developed finite element model of the overall bearing to investigate overall tension and torsion performance, the overall properties such as tension stiffness, yield strength, yield strain and limit deformation has great important reference for design and application of rubber bearing at tension state. Actually, there is a preformed hole in rubber bearings and the tensile stress distribution and deformation rule are different with that of the bearings without hole, moreover, the present numerical and experimental research mainly focuses on the tension properties but not on the cracking collapse mechanics (Zhang 2012), the cracking collapse mechanics of rubber bearings under tension loading need to be studied.

In order to predict the cracking collapse mechanics of rubber bearings, an analysis model is developed firstly in this paper for rubber bearings with preformed hole using a superposition approach, and then a tension model for analyzing the rubber layers is proposed based on the theory of elasticity, the stress and deformation expressions for the tensile rubber layer are derived applying the boundary restraint condition and the assumption of incompressibility of the rubber layer. Based on the derived expressions, the stress distribution and deformation pattern especially for the deformation shapers of the free edges of the rubber layer are analyzed and compared with the finite element analysis results. Furthermore, the theory of cracking energy is applied to analyze the distributions of cracking energy density and gradient direction, and the prediction of crack initiation and crack propagation direction of the rubber layers is investigated. Finally, the tests on the laminated rubber bearings under tensile loading are presented and the prediction results based on the theory of cracking energy are compared with the test results.

## 2. Analysis model of rubber layer

For the circular rubber bearing with a preformed hole, consider a rubber layer of the axial height h and outer radius a, inside radius b. The rubber layer is bonded to rigid end plates at $z$=0 and $z$=$h$ which prevent all distortions of its end surfaces. It is assumed throughout that the rubber layer is homogeneous and isotropic, and that during the subsequent deformations the displacement gradients are sufficiently small for the classical linear theory of elasticity to be applicable. The resulting deformation is calculated here by the superposition of the displacements arising in two separate specified loading situations (Zhang 2012), as represented diagrammatically in Fig. 1. Case A (uniform tension state): the rubber layer is subject to an axial tensile load and at the same time the outer and inside surfaces are prevented from distorting by the application of a tensile stress of magnitude $\sigma_L$. Case B (lateral tension state): the same rubber layer is loaded on its lateral

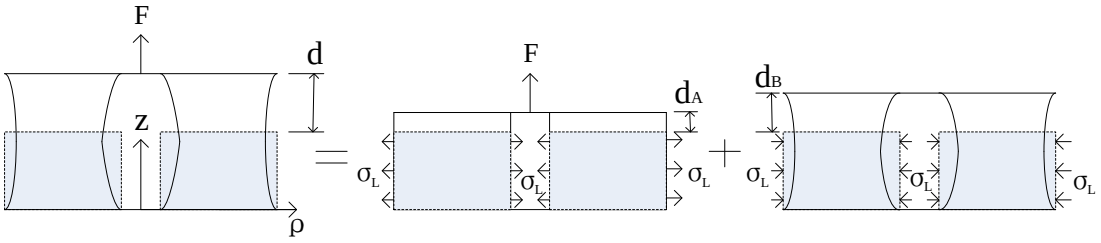


(C) (A) (B)

Fig. 1 Tension model of rubber layer

surfaces alone with a compressive stress equal and opposite to that in Case A.

Case A (uniform tension state): Suppose that the rubber layer is subjected to an axial tensile load $F$ which is applied on the plane end face $z=h$ with the lateral faces restrained to remain undistorted and parallel to the $z$-axis by tensile stresses of magnitudeσL applied normally to these faces. The magnitude of the imposed axial stress is $F/A$ and the material is everywhere in a state of hydrostatic tensile stress, whose magnitude $\sigma_L$ is given by

$$\sigma_L = \sigma = F / \pi(a^2 - b^2) \tag{1}$$

Case B (lateral tension state): the same rubber layer is loaded on its lateral surfaces by a radial compressive stress $-\sigma_L$, which are equal and opposite to those in Case A. The displacement and the corresponding strain and stress components at a point within the rubber are denoted by $u_i$, $\varepsilon_{ij}$ and $\sigma_{ij}$ respectively, with $i, j=\rho, \phi$ or $z$. The assumption of incompressibility implies that Poisson's ratio $\mu$=0.5 and shear modulus $G=E/3$, then the constitutive equations relating the stress and strain components become (Xu 2009)

$$\varepsilon_{\rho\rho} = [\sigma_{\rho\rho} - 0.5(\sigma_{\phi\phi} + \sigma_{zz})] / E = \frac{\partial u_\rho}{\partial \rho} \tag{2-1}$$

$$\varepsilon_{\phi\phi} = [\sigma_{\phi\phi} - 0.5(\sigma_{zz} + \sigma_{\rho\rho})] / E = \frac{u_\rho}{\rho} \tag{2-2}$$

$$\varepsilon_{zz} = [\sigma_{zz} - 0.5(\sigma_{\rho\rho} + \sigma_{\phi\phi})] / E = \frac{\partial u_z}{\partial z} \tag{2-3}$$

$$\varepsilon_{z\rho} = 3\sigma_{z\rho} / E = \frac{\partial u_\rho}{\partial z} + \frac{\partial u_z}{\partial \rho} \tag{2-4}$$

And the incompressibility condition implies that

$$\varepsilon_{\rho\rho} + \varepsilon_{\phi\phi} + \varepsilon_{zz} = \frac{\partial u_\rho}{\partial \rho} + \frac{u_\rho}{\rho} + \frac{\partial u_z}{\partial z} = 0 \tag{3}$$

Which upon integration gives

$$u_\rho = -\frac{\rho}{2}\frac{\partial u_z}{\partial z} + \frac{f(z)}{\rho} \tag{4}$$

With the function $f(z)$ depending upon $z$ alone. The force-free lateral surfaces will be drawn inwards, as illustrated in Fig. 1, suppose there is a position $\rho=\rho 0$, where the radial deformation is equal to zero, then

$$f(z) = \frac{\rho_0^2}{2}\frac{\partial u_z}{\partial z} = k\frac{\partial u_z}{\partial z} \tag{5}$$

Substituting the representation (5) into the representation (4)

$$u_\rho = (-\frac{\rho}{2} + \frac{k}{\rho})\frac{\partial u_z}{\partial z} \tag{6}$$

Since the loading is axisymmetrical and plane cross-sections normal to the z-axis are assumed to remain plane

$$u_\phi = 0\,,\ \frac{\partial u_\rho}{\partial \phi} = \frac{\partial u_z}{\partial \phi} = \frac{\partial u_z}{\partial \rho} = 0 \tag{7}$$

Substituting the representation (7) into the Eqs. (2-1)、(2-2)、(2-4) and (6) yields

$$\sigma_{\phi\phi} = \sigma_{\rho\rho} + \frac{4Ek}{3\rho^2}\frac{\partial u_z}{\partial z} \tag{8-1}$$

$$\sigma_{zz} = \sigma_{\rho\rho} + (1 + \frac{2k}{3\rho^2})E\frac{\partial u_z}{\partial z} \tag{8-2}$$

$$\sigma_{z\rho} = \frac{E}{3}\frac{\partial u_\rho}{\partial z} = (-\frac{\rho}{6} + \frac{k}{3\rho})E\frac{\partial^2 u_z}{\partial z^2} \tag{8-3}$$

According to the equilibrium equation which must be fulfilled in the radial direction (Xu 2009)

$$\frac{\partial \sigma_{\rho\rho}}{\partial \rho} + \frac{\partial \sigma_{z\rho}}{\partial z} + \frac{\sigma_{\rho\rho} - \sigma_{\phi\phi}}{\rho} = 0 \tag{9}$$

Substituting the representation (8) into the Equation (9) yields

$$\sigma_{\rho\rho} = (\frac{1}{12}\rho^2 - \frac{k\ln\rho}{3})E\frac{\partial^3 u_z}{\partial z^3} - \frac{2Ek}{3\rho^2}\frac{\partial u_z}{\partial z} + C \tag{10}$$

With the function $C$ can be determined by applying the boundary conditions imposed at lateral faces of the block, $\sigma_{\rho\rho}=-\sigma_L$ ($\rho=a, b$)

$$\sigma_{\rho\rho 1} = (\frac{1}{12}\rho^2 - \frac{1}{12}b^2 - \frac{k\ln(\rho/b)}{3})E\frac{\partial^3 u_z}{\partial z^3} - \frac{2Ek}{3}(\frac{1}{\rho^2} - \frac{1}{b^2})\frac{\partial u_z}{\partial z} - \sigma_L \quad (b<\rho<\rho_0) \tag{11-1}$$

$$\sigma_{\rho\rho 2}=(\frac{1}{12}\rho^2-\frac{1}{12}a^2-\frac{k\ln(\rho/a)}{3})E\frac{\partial^3 u_z}{\partial z^3}-\frac{2Ek}{3}(\frac{1}{\rho^2}-\frac{1}{a^2})\frac{\partial u_z}{\partial z}-\sigma_L \quad (\rho_0<\rho<a) \tag{11-2}$$

Substituting the representation (11-1, 11-2) into the Eqs. (8-2) yields

$$\sigma_{zz1}=(\frac{1}{12}\rho^2-\frac{1}{12}b^2-\frac{k\ln(\rho/b)}{3})E\frac{\partial^3 u_z}{\partial z^3}+(\frac{2Ek}{3b^2}+E)\frac{\partial u_z}{\partial z}-\sigma_L \quad (b\le\rho<\rho_0) \tag{11-3}$$

$$\sigma_{zz2}=(\frac{1}{12}\rho^2-\frac{1}{12}a^2-\frac{k\ln(\rho/a)}{3})E\frac{\partial^3 u_z}{\partial z^3}+(\frac{2Ek}{3a^2}+E)\frac{\partial u_z}{\partial z}-\sigma_L \quad (\rho_0<\rho\le a) \tag{11-4}$$

However, in this loading case, there is no axial force imposed and so $\int_b^{\rho_0}\sigma_{zz1}\rho d\rho+\int_{\rho_0}^{a}\sigma_{zz2}\rho d\rho=0$ Substituting the representation (11-3, 11-4) yields

$$W_1\frac{\partial^3 u_z}{\partial z^3}-W_2\frac{\partial u_z}{\partial z}+W_3=0 \tag{12}$$

where

$$W_1=\frac{E\rho_0^2}{12}(a^2-b^2)+\frac{E\rho_0^2}{12}\ln\frac{b}{a}-\frac{E}{48}(a^4-b^4)$$

$$W_2=\frac{Ek\rho_0^2}{3}(\frac{1}{a^2}-\frac{1}{b^2})-\frac{E}{2}(a^2-b^2)$$

$$W_3=-\sigma_L(a^2-b^2)/2$$

Since the rubber is assumed to be bonded to rigid end plates, $\frac{\partial u_z}{\partial z}|_{z=0,h}=0$ and $u_z|_{z=0}=0$, therefore, solution of Eq. (12) can be written as

$$u_z=\frac{W_3}{W_2}[z-\frac{2}{\beta}\sinh(\beta z/2)\cosh(\beta h/2-\beta z/2)/\cosh(\beta h/2)] \tag{13}$$

Where $\beta=\sqrt{W_2/W_1}$. On the other hand, $\sigma_{\rho\rho1}=\sigma_{\rho\rho2}$ at the position $\rho=\rho_0$, but it is difficult to precisely meet the condition all at the section, as a result, suppose $\sigma_{\rho\rho1}=\sigma_{\rho\rho2}$ at the key points $z$=0 or h. Therefore, $\rho_0$ can be obtained according to Eqs. (11-1) and (11-2)

$$\rho_0=\sqrt{2k}=\sqrt{0.5(a^2-b^2)/\ln(a/b)} \tag{14}$$

Substituting the representation (13) into the Eq. (6) yields

$$u_\rho=\frac{W_3}{W_2}(-\rho+\rho_0^2/\rho)[\sinh(\beta z/2)\sinh(\beta h/2-\beta z/2)/\cosh(\beta h/2)] \tag{15}$$

Finally, substituting the representation (13) into the Eqs. (11), (8-3) yields

$$\sigma_{\rho\rho 1}=\frac{W_3E}{W_2}[\frac{2k}{3\rho^2}-\frac{2k}{3b^2}-\frac{\beta^2(\rho^2-b^2)}{12}+\frac{k\beta^2\ln(\rho/b)}{3}]\frac{\cosh(\beta z-\beta h/2)}{\cosh(\beta h/2)}+\frac{2W_3Ek}{3W_2}(\frac{1}{b^2}-\frac{1}{\rho^2}) \quad (b\le\rho<\rho_0)$$

$$\sigma_{\rho\rho 2}=\frac{W_3E}{W_2}[\frac{2k}{3\rho^2}-\frac{2k}{3a^2}-\frac{\beta^2(\rho^2-a^2)}{12}+\frac{k\beta^2\ln(\rho/a)}{3}]\frac{\cosh(\beta z-\beta h/2)}{\cosh(\beta h/2)}+\frac{2W_3Ek}{3W_2}(\frac{1}{a^2}-\frac{1}{\rho^2}) \quad (\rho_0<\rho\le a) \quad (16\text{-}1)$$

$$\sigma_{zz1}=\frac{W_3E}{W_2}[-\frac{2k}{3b^2}-1-\frac{\beta^2(\rho^2-b^2)}{12}+\frac{k\beta^2\ln(\rho/b)}{3}]\frac{\cosh(\beta z-\beta h/2)}{\cosh(\beta h/2)}+\frac{W_3E}{W_2}(\frac{2k}{3b^2}+1) \quad (b\le\rho<\rho_0) \quad (16\text{-}2)$$

$$\sigma_{zz2}=\frac{W_3E}{W_2}[-\frac{2k}{3a^2}-1-\frac{\beta^2(\rho^2-a^2)}{12}+\frac{k\beta^2\ln(\rho/a)}{3}]\frac{\cosh(\beta z-\beta h/2)}{\cosh(\beta h/2)}+\frac{W_3E}{W_2}(\frac{2k}{3a^2}+1) \quad (\rho_0<\rho\le a) \quad (16\text{-}3)$$

$$\sigma_{z\rho}=\frac{W_3E\beta}{W_2}(\frac{\rho}{6}-\frac{k}{3\rho})\frac{\sinh(\beta z-\beta h/2)}{\cosh(\beta h/2)} \quad (16\text{-}4)$$

## 3. Results analysis

Based on the derived expressions, the stress distribution and deformation pattern especially for the deformation shapers of the free edges of the rubber layer can be analyzed. On the other hand, the finite element analysis result is adopted also to compare with the stress and deformation expressions. In this work we define a rubber layer with different shape factors, as shown in Fig. 2, the rubber layer is 6 mm thick and the different values of the shape factor are realized by defining different values of the outer diameter ($D$=300, 500), and the inside diameter $d$=40 mm. Suppose the rubber layer is made of natural rubber with the shear modulus G=0.4 MPa and the bulk modulus of elasticity $Eb$=200MPa. The finite element model is performed using the Abaqus code with the Mooney-Rivlin material model coefficients given by: $C$10=0.2, $C$01=0.005. Since the geometrical and loading conditions are axisymmetric, the finite element model is defined by axisymmetric elements. In order to avoid finite element size effect, different types of mesh are defined and analyzed, and one mesh consists of 500 elements in the radial direction and 10 elements in height direction is applied.

In Fig. 3 distribution of the axial stress, through longitudinal mid-height of the rubber layer with different shape factors, is plotted nondimensionalized with respect to the maximum tensile stress. The solid lines represent the theory solution results, the other curves represent the results

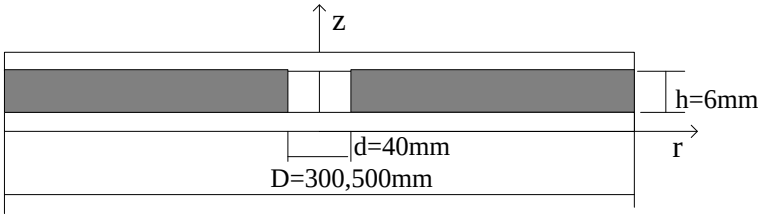


Fig. 2 Geometrical dimensions of rubber layers

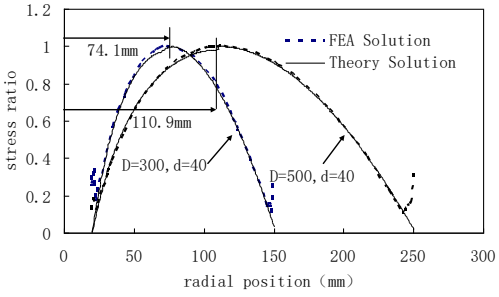


Fig. 3 Normal stress distribution in the radial direction

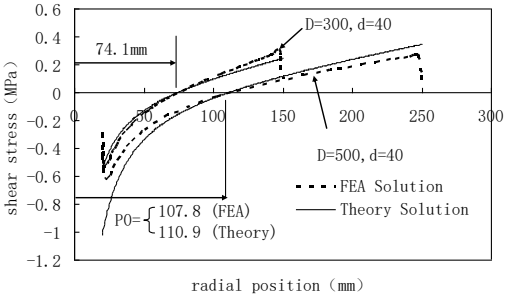


Fig. 4 Shear stress distribution in the bonded surface

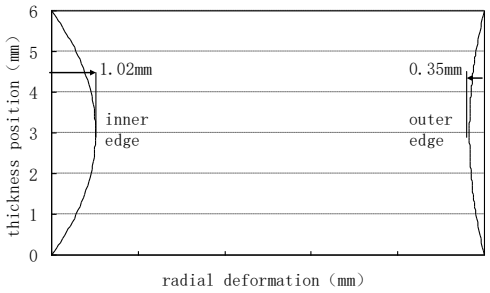


Fig. 5 Rubber layer deformation

provided by the numerical analysis referred to the different shape factor bearings. The results show that the normal stress decreases at the circumference of the rubber layer and the maximum normal stress position can be determined according to the normal stress results. On the other hand, the maximum normal stress position can also be calculated through the representation (14), which is 74.1 mm and 110.9 mm for both the rubber layers, respectively. Fig. 3 indicates that the correlation between the numerical solutions and the analytical ones is also quite good. It should be noted that stress concentrations are encountered in the region close to the edge according to the FE analysis results proposed by Imbimbo and Luca (1998), and the theoretical analysis can't simulate it. However, it is known that for a thin rubber layer block, the effect of the stress concentration is confined to a very narrow region near the circumference (Benthem 1972). Thus we expect the theoretical analysis method is suitable.

Fig. 4 shows the distribution of the horizontal shear stress on the bonded surface, through the longitudinal section of the rubber layer, for both the bearings with different shape factor respectively. The shear stress results refer to the part of the rubber layers placed at the interfaces with the steel shims. The analysis results show that the shear stress direction at the outer circumference of the bonded surface is opposite to that at the inner circumference of the bonded surface, and there is a neutral surface where the shear stress is equal to zero. The neutral surface radius can be calculated through representation (14), Figs. 3 and 4 indicate that the normal stress reaches a maximum and the shear stress becomes zero at $\rho$=74.1 mm and $\rho$=110.9 mm for both the rubber layers, respectively. The results show that the correlation between the numerical solutions and the analytical ones is very good except for the position around the lateral surfaces. The results of the theoretical analysis are relatively smooth, but the numerical results show that stress concentrations are encountered in the region close to the lateral edges of the rubber layer, which is

similar with the analysis results from Imbimbo and Luca (1998).

When the rubber layer is subjected to an axial tensile loading, the inner and outer lateral surfaces will be drawn inwards. Fig. 5 shows the deformation results of the lateral surfaces of the rubber layer with diameter $D$=500mm, the analysis results are calculated according to the representation (15), in which $\rho$=20 and 250, respectively. The results show that the deformation of the lateral edges of the rubber layer is approximate parabolic profile, and the deformation of the inner edge is larger than that of the outer edge.

## 4. Cracking prediction

Up to now, the crack collapse have been studied in many rubber components such as tires and hoses, but paid less attention in rubber bearings. Reasonable rubber material constitutive model and failure criterion is need to analyze the cracking mechanics of the rubber layer, Mars (2002) introduced a concept of cracking energy density to describe the crack initiation and propagation in rubber materials. The cracking energy density is defined as the energy produced by the principal stress acting directly on each crack, and the orientation of maximum cracking energy density is the direction of maximum principal tensile stress.

In this article, we aim at predicting the cracking initiation location and cracking direction but not the cracking process, because the real failure process is based on accurate rubber material constitutive model and failure criterion. The cracking energy density can be calculated as (Mars 2002)

$$W = r^T k_c^T [\int_0^{\varepsilon} \sigma d\varepsilon] kr \tag{17}$$

Where $r$ is a unit vector normal to the crack plane, $k_c$ is the transformation matrix from the crack plane to the principal stresses. The stress distribution of a rubber layer under tensile loading can be calculate through representation (16) in this paper, and then the principal stresses $\sigma_1$, $\sigma_2$ and $\sigma_3$ at any point of rubber layer can be determined. As a result, the cracking energy density due to the principal stresses can be calculated as following

$$W = (\sigma_1^2 - \nu\sigma_1\sigma_2 - \nu\sigma_1\sigma_3)/2E \tag{18}$$

Suppose that here are no intrinsic flaws in the rubber layer, and the crack will propagate toward the point of minimum strain energy density around the crack tip, which is utilized to determine the direction of crack propagation. As a result, the crack in bonded rubber layer initiates at the point with the maximum cracking energy density, and then propagates along the direction with the lowest cracking energy density.

Rubber layer with different outer diameters are analyzed under tensile load equivalent to 0.1 MPa. To compare their cracking performance, the contours of cracking energy densities in rubber layers with outer diameter $D$=100, and inner diameter $d$=40, 20 are shown in Fig. 6 and Fig. 7, respectively. The position with the maximum cracking energy density in Fig. 6 is located at the mid-cross-section of the layer and 31mm from the center axis, which indicates that the crack is most likely to initiate here. However, Fig. 7 representing the other rubber layer ($D$=100, $d$=20) shows that the maximum cracking energy density occurs at the inner surface between rubber layer and steel plates, where the crack is most likely to initiate. As a result, the crack initiation location is different for different rubber layers.

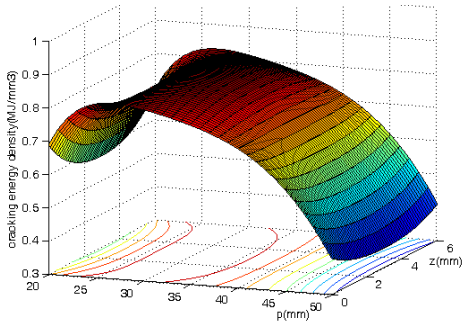


Fig. 6 Cracking energy density distribution in rubber layer ($D$=100 $d$=40)

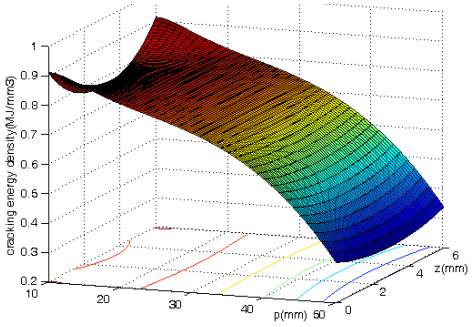


Fig. 7 Cracking energy density distribution in rubber layer ($D$=100 $d$=20)

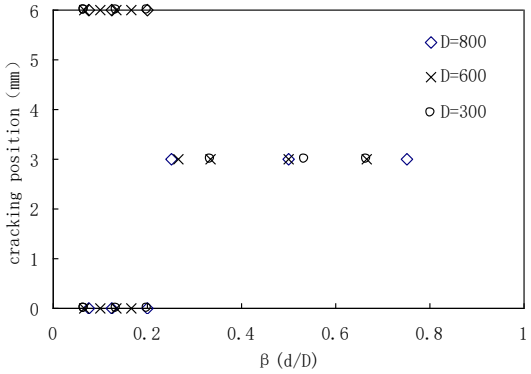


Fig. 8 Crack position in the thickness direction

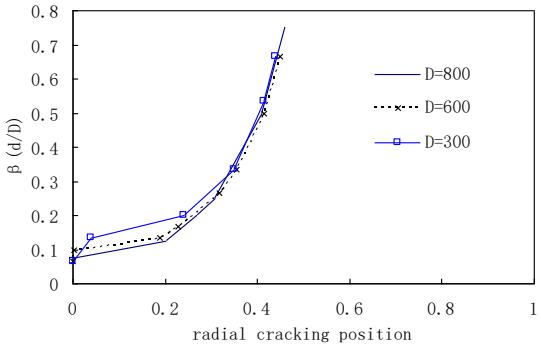


Fig. 9 Crack position distribution in the radial direction

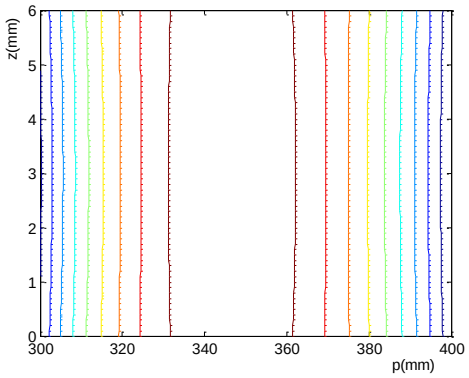


Fig. 10 Cracking energy density gradient distribution ($D$=800 $d$=600)

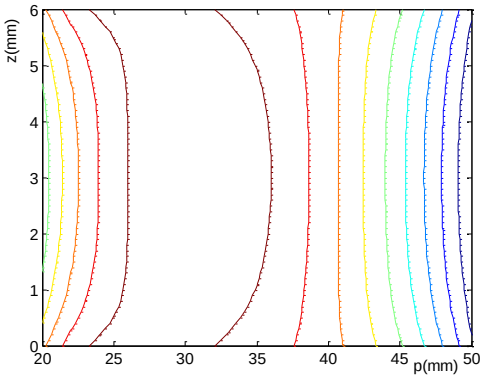


Fig. 11 Cracking energy density gradient distribution ($D$=100 $d$=40)

Initial cracking position of rubber layer in the thickness direction with different outer diameters $D$=800, 600, 300 mm and different aperture ratio $\beta$=0.05~0.75 are show in Fig. 8. The results show that the crack initiate at the inner surface between rubber layer and steel plates for rubber layer with aperture ratio $\beta$ <0.2, and the crack initiate at the mid-height of the layer for rubber layer with aperture ratio $\beta$ >0.2. Fig. 9 represents the distribution of initial cracking position of rubber layer

in the radial direction. It can be seen from the figure that initial cracking position gradually moves to the inner surface with the aperture ratio decrease.

After the initial cracking position is determined, the crack propagation direction can be estimated by the distribution of cracking energy density gradient. Fig.10and Fig.11 represent the distribution of cracking energy density gradient for two kinds of rubber layers respectively, which show that the direction of cracking energy density gradient is almost horizontal, and it is approximately right for other cases.

## 5. Experimental results analysis

Tensile tests on three groups of ordinary laminated rubber bearing are carried out to study the cracking mechanics of the rubber bearing (Zhang 2012). Pure tension test, shear-tension test and tension-shear test are performed on the three groups, and each group consists of nature laminated rubber bearings and lead core rubber bearings. The first group includes two ordinary laminated rubber bearings with 800mm diameter (LNR-1 and LRB-1), which is tested under pure tensile load. Fig. 12 shows the geometrical dimensions of the rubber bearing, each bearing is made of twenty-six rubber layers, each rubber layer is 6 mm thick and each steel shim is 3.5 mm thick. The shear modulus is 0.40 Mpa, the first shape factor is 30.83, and the second is 5.13. The test setup is shown in Fig. 13. The vertical load is controlled through a 2000 kN vertical jack, and the maximum vertical displacement stroke is 600 mm.

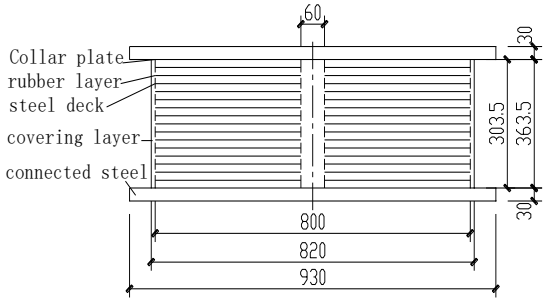


Fig. 12 Geometrical dimensions of rubber bearings

Fig. 13 Rubber bearing test

Fig. 14 Crack of the rubber layer for LNR-1


Fig. 15 Crack of the rubber layer for LRB-1

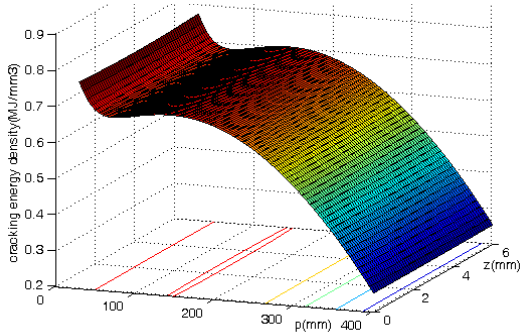


Fig. 16 Cracking energy density distribution in the rubber layer

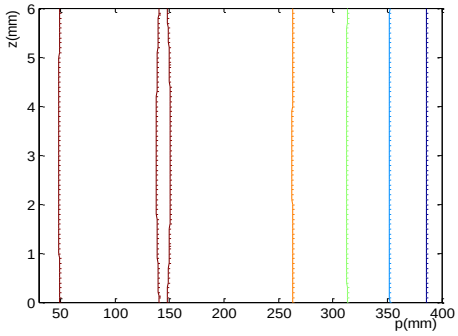


Fig. 17 Cracking energy density gradient distribution

Vertical hysteresis tension test is performed when the vertical tensile strain reaches 10%, and then the rubber bearing is stretched to failure. The sound can be hear during the stretch, which may be due to the rubber tearing or cracking of adhesive layer, and it is especially obvious for the lead rubber bearing. The first rubber bearing ruptures suddenly, and the cracking surface is located between rubber layer and steel plates as shown in Fig. 14, and there are some rubber residues on the plate. For the lead rubber, an obvious tearing crack emerges in the protective rubber layer around the bearing (Fig. 15), it is found that much of this rubber layer in the rubber bearing has been break and some rubber residues on the steel plate.

The cracking behavior is also predicted by the method of cracking energy density, the contour of cracking energy densities in the rubber layer is shown in Fig. 16, and the distribution of cracking energy density gradient is shown in Fig. 17. The analysis results show that the maximum cracking energy density occurs at the inner surface between rubber layer and steel plates and the crack is predicted to initiate there, and develops rapidly in the horizontal direction until the fracture of the overall cross-section of the rubber layer, which is consistent with the experimental phenomenon approximately.

## 6. Conclusions

In order to study the cracking performance of laminated rubber bearings under tensile loading, a tension model for analyzing the rubber layers is developed and the stress and deformation expressions for the tensile rubber layer are derived and analyzed in this paper. Based on the derived expressions, the theory of cracking energy is applied to analyze the distributions of cracking energy density and gradient direction. The crack initiation, crack propagation direction and failure mechanism of the rubber layers are investigated, the following conclusions or recommendations can be made:

• The stress and deformation expressions are based on the equilibrium equations and the incompressibility constraint, as a result, the results is suitable to rubber bearings under low tensile load. The position of the maximum normal stress in the rubber layer can be determined through the representation (14). The deformation of the lateral edges of the rubber layer is approximate parabolic profile, and the deformation of the inner edge is larger than that of the outer edge. The stress and deformation expressions maybe not suitable in the nonlinear stage, but the initial

stiffness, cracking point, and other failure mechanism can still be predicted.

• Shape factor and aperture ratio are main factors which affect the stress distribution and deformation of the rubber layer.

• The crack energy method is feasible to analyze cracking initiation and cracking direction of rubber layer under tensile loading, the crack initiation location and the crack propagation direction can be approximately predicted by the distribution of cracking energy density and gradient of the rubber layer under low tensile load. The analysis results show that aperture ratio plays an important role on the crack initiation location, the crack initiate at the inner surface between rubber layer and steel plates for rubber layer with aperture ratio $\beta$<0.2, and the crack initiate at the mid-height of the layer for rubber layer with aperture ratio $\beta$>0.2.

• The experimental results show the cracking failure of the rubber layer, the predicted results on the cracking mechanism is consistent with the experimental phenomenon, and the crack energy method can be used to approximately predict the cracking initiation and propagation.

## Acknowledgments

The research described in this paper was financially supported by the Natural Science Foundation (50978009, 51278516) and Beijing Science and Technology Foundation (KM201210005025).

## References

Benthem, J.P. and Minderhoud, P. (1972), "The problem of solid cylinder compressed between rough rigid stamps", *Int. J. Solid. Struct.*, **8**, 1027-1042.

Hino, J., Yoshitomi, S. and Tsuji, M. (2008), "Bound of aspect ratio of base-isolated buildings considering nonlinear tensile behavior of rubber bearing", *Struct. Eng. Mech.*, **30**(3), 351-368.

Imbimbo, M. and Luca, A.D. (1998), "FE stress analysis of rubber bearings under axial loads", *Comput. Struct.*, **68**, 31-39.

Jain, S.K. and Thakkar, S.K. (2005), "Experimental investigations on laminated rubber bearings", *Bull Earthq. Eng*, **3**(1), 129-136.

Kilar, V. and Koren, D. (2009), "Seismic behavior of asymmetric base isolated structures with various distributions of isolators", *Eng. Struct*, **31**(4), 910-921.

Lee, H.P., Cho, M.S., Kim, S.Y., Park, J.Y. and Jang, K.S. (2014), "Experimental study on the compressive stress dependency of full scale low hardness lead rubber bearing", *Struct. Eng. Mech.*, **50**(1), 089-103.

Ling, Y., Engel, P.A. and Brodsky, W.L. (1995), "Compression of bonded annular rubber blocks", *J. Eng. Mech.*, **121**(6), 661-666.

Liu, W.G., Yang, Q.R. and Zhou, F.L. (2004), "Nonlinear elastic rotation and shear property theoretical and experimental research of rubber isolators", *Earthq. Eng. Eng. Vib.*, **24**(2), 158-167.

Mars, W.V. (2002), "Cracking energy density as a predictor of fatigue life under multiaxial conditions." *Rub. Chem. Technol.*, **75**, 1-17.

Matsuda, A. (2004), "Evaluation for mechanical properties of laminated rubber bearings using finite element analysis", *J. Press. Ves. Tech.*, **126**, 134-140.

Melkumyan, M.G. (2013), "New approach in design of seismic isolated buildings applying clusters of rubber bearings in isolation systems", *Eartq. Struct.*, **4**(6), 587-606.

Mosqueda, G., Masroor, A., Sanchez, J. and Ryan, K. (2010), "Performance Limit States of Seismically Isolated Buildings with Elastomeric Bearings", *Proceedings from the 9th US National and 10th Canadian*

*Conference on Earthquake Engineering*, Toronto, Canada, July.
Muramatsu, Y., Nishikawa, I. and Kawabata, I. (2001), "Tensile property of large-sized natural rubber bearing", *AIJ J. Tech.*, **12**, 53-56.
Sarno, L.D., Chioccarelli, E. and Cosenza, E. (2011), "Seismic response analysis of an irregular base isolated building", *Bull Earthq. Eng.*, **9**, 1673-1702.
Takaoka, E., Takenaka, Y. and Nimura, A. (2011), "Shaking table test and analysis method on ultimate behavior of slender base-isolated structure supported by laminated rubber bearings", *Earthq. Eng. Struct. Dyn*, **40**, 551-570.
Warn, G.P. and Whittaker, A.S. (2008), "Vertical stiffness of elastomeric and lead-rubber seismic isolation bearings", *J. Struct. Eng.*, **133**(9), 1227-1236.
Xu, L. and Wu, G.Z. (1999), "Some forms of strain energy function for rubber with finite element analysis", *Rub. Indust.*, **46**(12), 707-711.
Xu, Z.L. (2009), *A concise course in elasticity*, Higher education press, Beijing.
Yang, Q.R., Liu, W.G., He, W.F. and Feng, D.M. (2010), "Tensile stiffness and deformation model of rubber isolators in tension and tension-shear states", *J. Eng. Mech.*, **136**(4), 429-437.
Yoshida, J., Abe, M. and Fujino, Y. (2004), "Three-dimensional finite-element analysis of high damping rubber bearings", *J. Eng. Mech.*, **130**(5), 607-620.
Zhang, Z.Q. (2012), "Tension property of laminated rubber bearings under tensile loading", Ph.D. Dissertation, Beijing University of Technology, Beijing, China.

## Notations

| | |
|---|---|
| $E$ | compression modulus of the rubber |
| $G$ | shear modulus of the rubber |
| $h$ | height of the rubber layer |
| $a$ | outer radius of the rubber layer |
| $b$ | inside radius of the rubber layer |
| $F$ | axial tensile load |
| $\sigma_L$ | equivalent tensile stress at the outer and inside surfaces |
| $\mu$ | poisson's ratio |
| $u_i$ $\varepsilon_i$ $\sigma_{ij}$ | displacement and the corresponding strain and stress components |
| $k_c$ | transformation matrix from the crack plane to the principal stresses |